Pinaki P. Bhattacharjee[a], Nobuhiro Tsuji[b]
[a] Department of Materials Science and Engineering, Indian Institute of Technology Hyderabad, Ordinance Factory Estate, Yeddumailaram, India
[b] Department of Materials Science & Engineering, Graduate School of Engineering, Kyoto University, Yoshida, Honmachi, Sakyo-ku, Kyoto, Japan

Development of highly cube textured nickel superconductor substrate tapes by Accumulative Roll Bonding (ARB)

Development of cube texture ($\{001\}\langle100\rangle$) has been investigated in pure Ni (99.97 %) deformed to ultrahigh straining ($\varepsilon = 6.4$) by accumulative roll bonding and then annealed at different temperatures for use as coated superconductor substrate. The as accumulative roll bonding processed sheets reveal a typical pure metal or copper type homogeneous deformation texture. After annealing at different temperatures, strong cube texture formation is observed and a nearly 100 % cube textured tape with almost twin-free microstructure is obtained after annealing at 800 °C for 1 h. The development of a sharp cube texture is accompanied by the development of a predominantly low angle boundary network. The very sharp cube texture formation in this material appears to be due to the oriented nucleation of cube grains at early stages of recrystallization and selective growth of these grains with progressing recrystallization. The results obtained indicate that accumulative roll bonding could be a very attractive route for fabricating highly cube textured superconductor substrate tapes from Ni.

Keywords: Nickel; Severe plastic deformation; Recrystallization; Texture; EBSD

1. Introduction

Nickel and nickel-base alloys are candidate materials for use as highly cube textured ($\{001\}\langle100\rangle$) coated superconductor substrates as shown in the Rolling Assisted Biaxially Textured Substrates (RABiTS™) method [1]. The very sharp cube texture required for the substrate material is generated by appropriate thermomechanical treatment comprising of a high degree of deformation (≥95 % reduction in thickness) by cold rolling followed by annealing. High temperature superconductor (HTS) layers with intermediate ceramic buffer layers are subsequently epitaxially grown on these cube textured substrates. The very sharp cube texture of the substrate materials ensures that the grain boundary network consists of low angle grain boundaries (LAGB) only so that when the HTS layers are epitaxially grown on these substrates they also have predominantly LAGB boundary network. The presence of a low angle boundary network in the epitaxial superconductor layer is absolutely necessary to achieve high critical current density. This is due to the fact that high angle boundaries act as typical "weak links" in the superconductor films and thereby reduce the critical current density values greatly [2].

One of the key requirements for enhancing the cube texture in the substrate material is to impart a very high amount of rolling reduction, as the amount of deformation is known to affect the quality and sharpness of the cube texture greatly [3]. A majority of the investigations aiming to develop appropriate thermomechanical treatments for optimizing the cube texture in the substrate material use conventional cold rolling in the processing cycle. However, it is generally difficult to achieve very high degrees of deformation (>99 % reduction in thickness) in conventional cold rolling due to the decreasing thickness of the sheets. A novel way to overcome this difficulty is to employ accumulative roll bonding (ARB) which is a severe plastic deformation technique based on rolling deformation for obtaining bulk ultrafine to nanostructured materials [4]. In the ARB process the starting thickness of the sheet materials remains constant during the rolling process so that arbitrarily high deformation level can be attained without using smaller diameter rolls or any additional requirement.

The current work explores the possibility of employing ARB processing for preparing highly textured Ni substrates for coated superconductor applications which have not been investigated previously. Detailed microstructural and textural characterizations have been done at different length scales using X-ray diffraction (XRD) and electron back scatter diffraction (EBSD) for quantifying the texture and understating the origin of cube texture in ARB processed Ni.

2. Experimental

As-received Ni plates (160 mm (length) × 62 mm (width) × 10 mm (thickness)) of purity 99.97 % were initially cold rolled to ∼80 % reduction in thickness using a laboratory scale two-high rolling mill having a roll diameter of 310 mm. Samples of ∼150 mm in length were then cut from the cold rolled sheets and annealed at 600 °C for 1 h

Note: The authors have opted to publish the print version of this paper in black and white; a colour version is available online at www.ijmr.de

in a vacuum furnace. The fully annealed sheets with thickness of 2 mm were used as the starting material for the subsequent ARB processing. The ARB process was carried out at room temperature using machine-oil lubrication. The first cycle of the ARB process consisted of just cold rolling the annealed sheets to ~50% reduction ($\varepsilon = 0.8$) in thickness (~1 mm). At the start of the second cycle the cold rolled sheets of 1 mm thickness were cut into two, degreased with acetone and wire brushed. The degreased surfaces of the two sheets were stacked, fixed together by spot welding at the ends and again cold rolled to 50% reduction in thickness. This process was repeated for each subsequent cycles up to 8 cycles ($\varepsilon = 6.4$). A constant roll peripheral speed of 17 m min^{-1} was used in all cases. The roll bonded sheets coming out from the exit side were immediately quenched in cold water to arrest any rise in temperature of the sheets. The ARB process described above is typically adopted for a range of materials [4].

The ARB processed materials were subsequently annealed at temperatures ranging from 300 to 800 °C for 1 h. In addition, some of the deformed samples were annealed at 300 °C for different lengths of time to observe the evolution of texture with progressing recrystallization.

Bulk texture analysis through XRD was carried out using a Philips X'pert texture goniometer from the rolling plane section (RD–TD plane, where RD and TD are the rolling and transverse directions, respectively). Four incomplete pole figures, {111}, {200}, {220} and {311} were measured and the orientation distribution function (ODF) was calculated from the pole figures by the arbitrarily defined cells (ADC) method [5] assuming orthorhombic sample symmetry.

In all cases microtexture was carefully characterized by using an automated EBSD unit attached to a FEI-SIRON scanning electron microscope (SEM) equipped with field emission gun (FEG). The EBSD maps were taken from the longitudinal sections (ND–RD planes, where ND and RD are normal and rolling directions of the sheets, respectively) as well as the rolling plane sections. In order to evaluate the through thickness texture homogeneity of the deformed sheets, EBSD scans were done at different thickness locations (defined by t/t_0, where t and t_0 are the thickness location of EBSD scan and thickness of the sheets, respectively), i.e., 0.125 (close to surface) and 0.375 (close to center). TSL-OIM™ software was used for the analysis of the microtexture data. Samples for the microtexture measurements were prepared by mechanical polishing with colloidal silica followed by electropolishing at room temperature using a mixture of acetic and perchloric acids (1 : 19 by volume) as the electropolishing reagent. A tolerance angle of 15° around the ideal locations in the orientation space was used to determine the volume fraction of individual texture components. A very fine step size of 50 nm was used for the fully deformed and partially recrystallized samples. The scanned area measured 25 μm × 30 μm for a single EBSD scan. For recrystallized sample a coarser step size of 1.50 μm was used to cover large scan area measuring 500 μm × 500 μm in a single scan.

3. Results

Figure 1 shows the microstructure and texture of the starting material used for the ARB processing. The orientation map shown in Fig. 1a show the spatial distribution of the

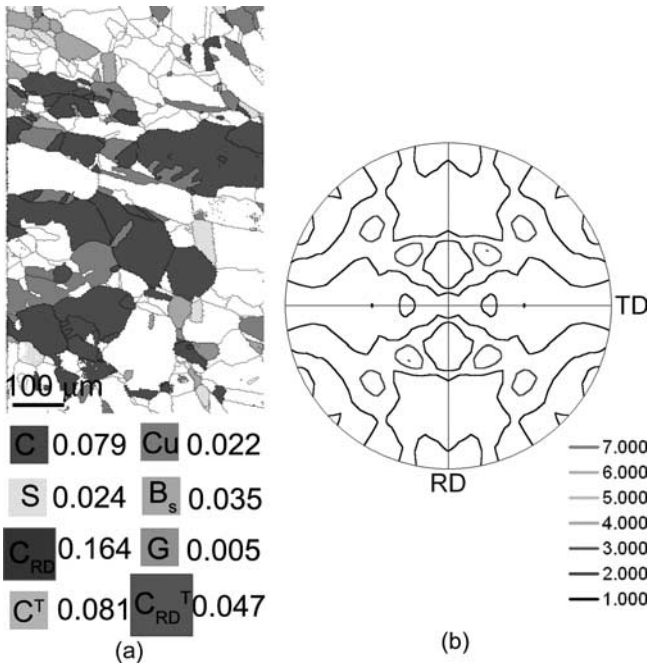

Fig. 1. (a) Orientation map and (b) (111) pole figure of the starting material for the ARB processing. The legends are the color codes for different texture components along with their respective volume fractions. (Colour online)

different texture components in the starting recrystallized sheet using different colors such as cube (C, blue), copper ({112}⟨111⟩, Cu, red), S ({123}⟨634⟩, yellow), brass ({110}⟨112⟩, B_s, green), RD-rotated cube ({100}⟨013⟩, C_{RD}, purple), Goss ({110}⟨001⟩, G, orange), cube-twin ({221}⟨122⟩, C^T, gray) and RD-rotated cube twin (C^T_{RD}, brown) along with their respective volume fractions indicated beside the color codes. The black lines in Fig. 1a show high angle grain boundaries (HAGBs, $\theta_{misorientation} \geq 15°$) and gray lines show the LAGBs ($2° \leq \theta_{misorientation} \leq 15°$). The texture of the starting material is found to be a weak and diffuse cube texture as may be seen from the orientation map and (111) pole figure shown in Fig. 1a and b, respectively. The average grain size is determined to be ~28 μm from a liner intercept analysis from the map shown in Fig. 1a.

Figure 2 shows the development of texture measured by XRD in the material ARB processed for 8 cycles ($\varepsilon = 6.4$). Figure 2a shows the (111) pole figure while Fig. 2b shows the relevant ODF sections ($\Phi_2 = 0°, 45°$ and 65°) along with the ideal locations for the typical rolling texture components such as cube (C), Copper (Cu), S, Brass (B_S), and Goss (G). The pole figure and ODF suggest the development of a typical pure metal or copper type deformation texture in the ARB processed material.

Figure 3 shows the development of microstructure and microtexture of the deformed material after 8 cycles of ARB processing measured by EBSD at different thickness locations. Figure 3a and 3b corresponds to the near surface ($t/t_0 = 0.125$) while Fig. 3c and 3d corresponds to the near center regions ($t/t_0 = 0.375$) of the as deformed sheet. Figure 3a and c shows the GB maps, and Fig. 3b and d the orientation maps. The microstructure of the as deformed material viewed in the longitudinal section (ND–RD plane) appears to be a lamellar boundary structure subdivided by

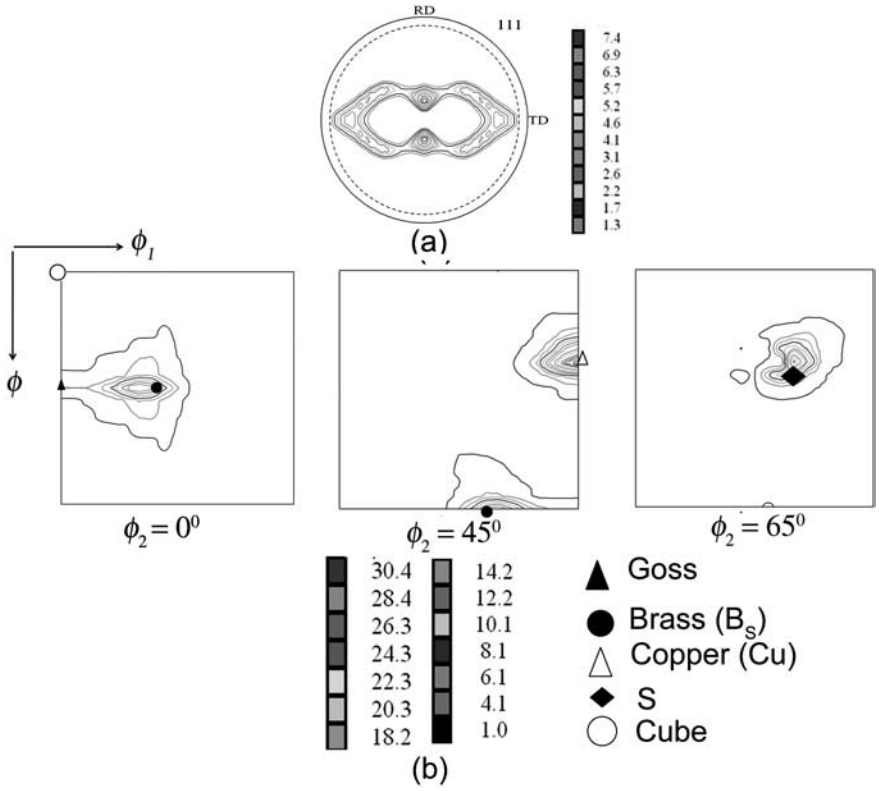

Fig. 2. (a) (111) pole figure and (b) $\Phi_2 = 0^\circ$, 45° and 65° sections of the ODF (measured by XRD) of the 8 cycles processed ARB sheet. Ideal locations of rolling texture components are shown in different ODF sections. (Colour online)

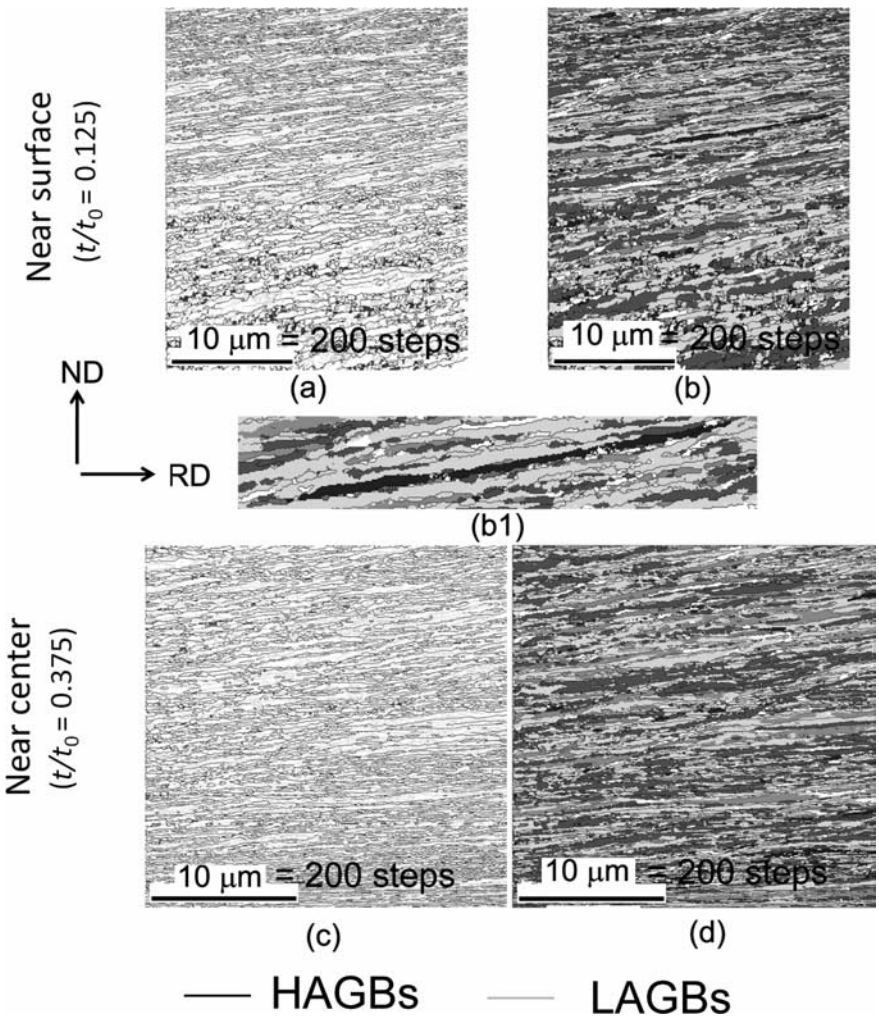

Fig. 3. (a) and (b) are GB and orientation maps of near surface region; (c) and (d) are corresponding maps for the near center region of the specimen ARB processed by 8 cycles. (b1) gives a magnified view of a region of interest in (b) showing a thin elongated cube band centered on $\{013\}\langle 100\rangle$ orientation. The color code for the orientation is same as in Fig. 1a. All data have been acquired through EBSD. (Colour online)

HAGBs typically observed in heavily cold rolled materials [6, 7]. The orientation maps indicate that the individual bands belong to different rolling texture components. Strong presence of the S (yellow) and Cu (orange) orientations could easily be detected in the orientation maps of different thickness locations (Fig. 3b and e). However, cube oriented (blue) regions could hardly be observed in the microstructure. Only in a part of the orientation map of the near surface region (Fig. 3b), a thin band could be detected (indicated by the arrow mark), which is reproduced in Fig. 3b1 for clarity. The cube band has an RD-rotated cube orientation (C_{RD}, $\{013\}\langle100\rangle$, purple) at one end of the band and gradually changes to the near cube orientation (blue) at other end. The band is several micrometers in length along RD but having an average thickness of only 300 nm.

Figure 4 shows the quantitative microtexture analyses corresponding to the EBSD maps at different thickness locations of the 8-cycle ARB processed specimen and compares it to 95 % straight rolled materials to elucidate the textural changes happening at such a high level of straining. Figure 4a shows the $\Phi_2 = 0^\circ$, 45° and 65° sections of the ODFs at two different thickness locations. The corresponding ODF sections of different thickness location appear very similar to each other and also bear good resemblance with the ODF obtained from bulk texture analyses (Fig. 2b). The volume fractions of typical rolling texture components at different thickness locations including the cube component have been shown and compared with 4-cycleARB processed and 95 % straight rolled materials in Fig. 4b. The main deformation texture components in the 8-cycleprocessed material are Cu ($\sim$27 % and 26 % at near surface and center locations, respectively), S ($\sim$48 % and 44 % at near surface and center locations, respectively) and the Bs components ($\sim$10 % and 15 % near surface and center locations, respectively). It may thus be clearly seen that remarkable through thickness homogeneity of texture is achieved in the 8-cycleprocessed material. As may also be observed from Fig. 4b that there are no major differences between the deformation textures of the 8-cycleprocessed material with that of straight rolled material. The major deformation texture components in all cases are the Cu, S and B_s components while cube (< 1 % in all cases), rotated cube and Goss components have negligible presence. The volume fractions of different texture components are found to vary between the three materials. The 8-cycleprocessed material appears to have slightly higher volume percentage of Cu component ($\sim$27 %) in contrast to the 95 % straight rolled materials ($\sim$15 %). The quantitative texture analyses at different length scales by EBSD and XRD clearly indicate that the deformation texture of the ARB processed material is a homogeneous pure metal or Cu type deformation texture and there are no significant but only gradual differences with the straight rolled material.

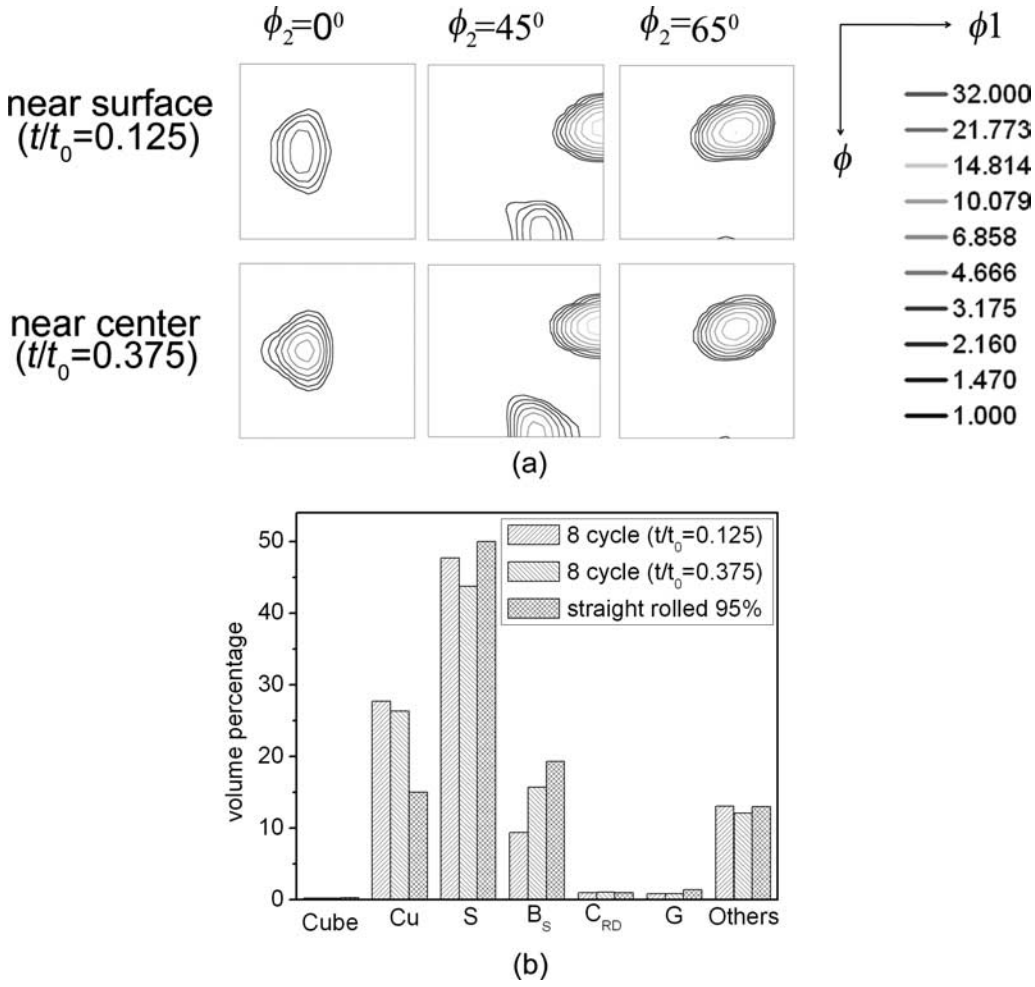

Fig. 4. (a) $\Phi_2 = 0^\circ$, 45° and 65° sections of the ODFs of near surface and center regions of the 8-cycle ARB processed sheet (colour online) and (b) plot showing the volume fraction of typical rolling texture components at different thickness locations.

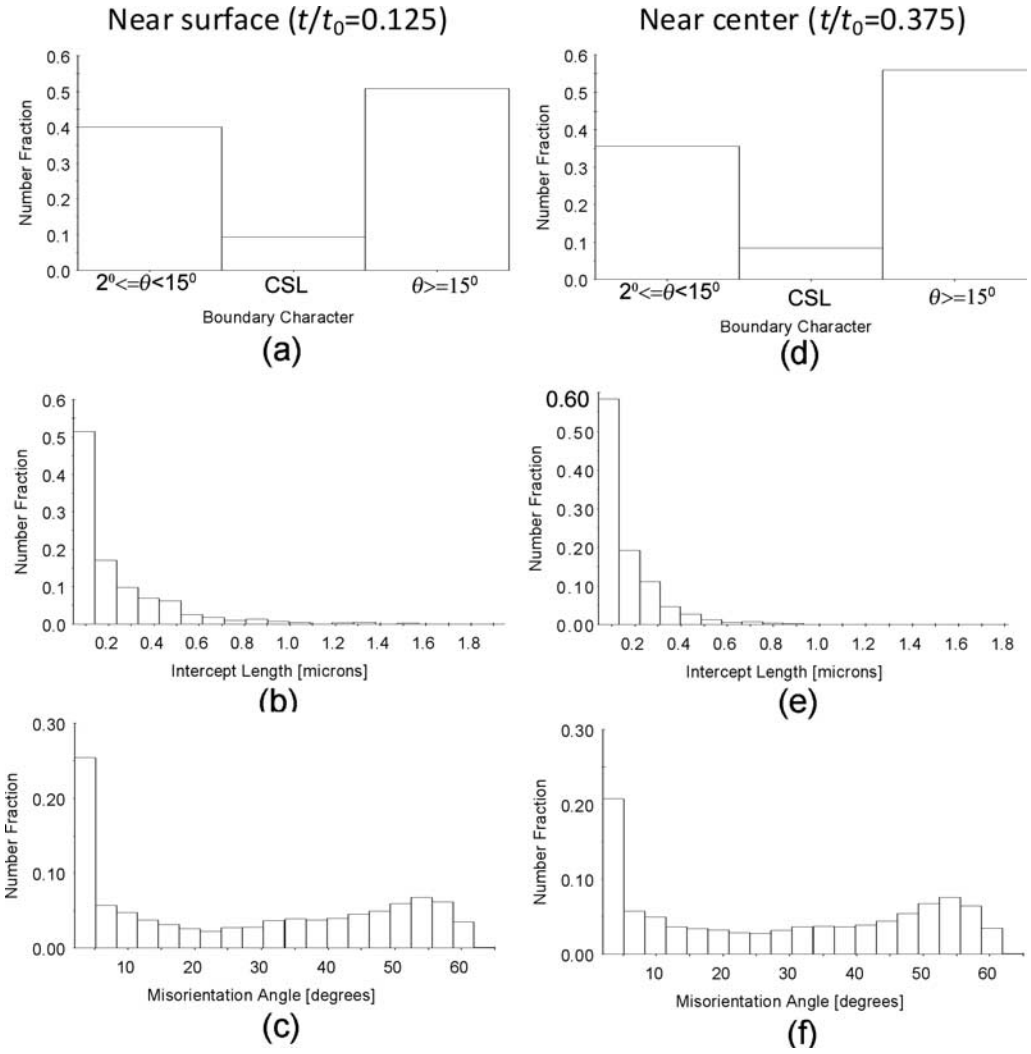

Fig. 5. (a), (b) and (c) are the GBCD, HAGB spacing and boundary misorientation plots for the near surface region of the specimen ARB processed by 8 cycles. (d), (e) and (f) are corresponding plots for the near center region.

The distribution of key microstructural parameters for adequately describing the lamellar structures of the sheets ARB processed for 8 cycles, such as fraction of high angle boundaries (f_{HAGB}), high angle boundary spacing ($d^{\mathrm{ND}}_{\mathrm{HAGB}}$) or the intercept length between HAGBs and misorientation angle (θ) for different thickness locations, are shown in Fig. 5. Figure 5a–c corresponds to the near surface region while Fig. 5d–f corresponds to the center region. Figures 5a and d show the grain boundary character distribution (GBCD), Fig. 5b and 5e shows the distribution of HAGB spacing and Fig. 5c and f shows the misorientation angle distribution of the corresponding regions. The fraction of HAGBs (including coincidence site lattice (CSL) boundaries which are also high angle boundaries) at the near surface region is 0.60 while at the center region the fraction is 0.64. The distributions of high angle boundary spacing at both thickness locations (Fig. 5b and 5e) show that a large fraction of boundary spacing lies between 100–200 nm. The average HAGB spacing at the near surface and central regions are found to be ~210 nm and 150 nm, respectively. From the misorientation distribution plots in Fig. 5c and 5f the average misorientation angles at near surface and near center regions are found to be 27° and 28°, respectively. Large area measurement with finer scan step size should render the values of key structural parameters calculated from the EBSD data statistically reliable within the angular resolution limit of EBSD measurement.

Table 1. Comparison of key structural parameter values in ARB and conventionally processed materials.

Material		f_{HAGB}	$d^{\mathrm{ND}}_{\mathrm{HAGB}}$ (nm)	Θ_{HAGB}
ARB processed	$t/t_0 = 0.125$	0.60	210	28°
	$t/t_0 = 0.375$	0.64	150	29°
95 % cold rolled conventionally processed		0.50	500	24°

The key microstructural parameters in the 8-cycleARB processed material have again been compared with 95 % straight rolled materials in Table 1. Much finer microstructure developed due to ARB processing is quite evident from the table. Based on EBSD and TEM studies (not provided here) at different stages of ARB processing the microstructure is found to continue to refine up to 8 ARB cycles and no microstructural saturation effect in terms of grain size or high angle boundary spacing has been observed up to this strain level.

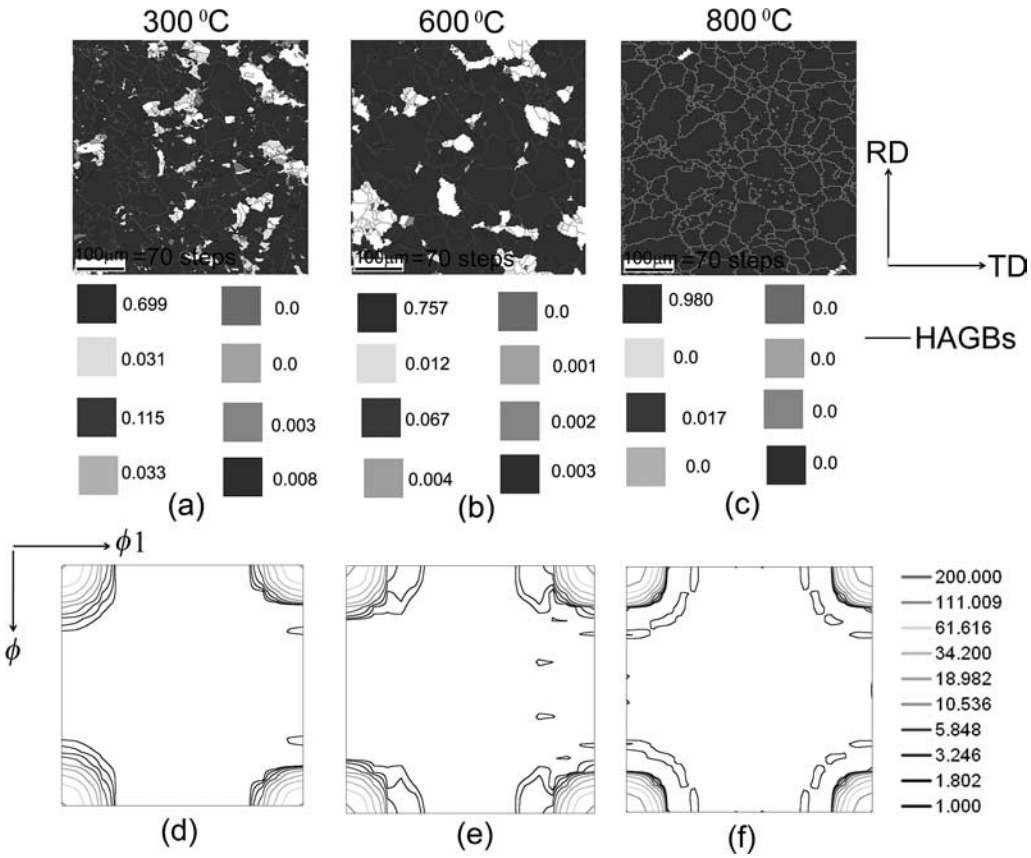

Fig. 6. Orientation maps (RD–TD section) of the 8-cycle ARB processed material after annealing at (a) 300, (b) 600 and (c) 800 °C. The color code for the orientation is same as in Fig. 1a. d, e and (f) are the $\Phi_2 = 0^\circ$ sections of the ODFs corresponding to 300, 600 and 800 °C annealed conditions. (Colour online)

Figure 6 shows the development of texture in the ARB processed sheets after annealing at different temperatures. Figure 6a and b corresponds to 300 °C, Fig. 6c and d corresponds to 600 °C and Fig. 6e and f corresponds to 800 °C annealing conditions. Figure 6a, c and e shows the orientation maps and Fig. 6b, d and f shows the $\Phi_2 = 0^\circ$ sections of the ODFs. Upon annealing at 300 °C (Fig. 6a) a strong cube texture is already developed in the material, which is quite evident from the volume fraction of the cube component ~0.70 and the intensity maxima (~117) in the corresponding ODF (Fig. 6b). The recrystallized grain size in this condition is ~24 μm. By annealing at 600 °C the cube volume fraction increases to ~76 % (Fig. 6c) and the intensity maxima of the ODF is also increased to ~130 (Fig. 6d). The recrystallized grain size in this condition is ~35 μm. Upon further annealing at 800 °C a nearly 100 % cube texture is observed (Fig. 6e). The ODF intensity in this annealed condition (Fig. 6f) reaches a very high value ~200. The average recrystallized grain size is in this condition is ~40 μm.

The quality and sharpness of the cube texture in the 800 °C annealed specimen is further analyzed in Fig. 7. The orientation map corresponding to the 800 °C annealed condition (Fig. 6 e) is reproduced in Fig. 7a with the cube grains shown in different colors depending on the misorientation from the exact cube location. The volume fractions of cube regions with misorientation less than 5° (blue), between 5° – 10° (dark blue) and between 10° – 15° (black) are found to be 34.5 %, 55.7 % and 9.5 %, respectively. The sharpness of the cube texture developed in the annealed tape can further be analyzed with the pole plot data (Fig. 7c) which shows the alignment of the ND with crystallographic [100] direction. The strong peak at 3.6° is due to the sharp alignment of [100] direction with the ND. The smaller peak near 90° is due to the symmetrical variants of [100] direction. If a [100] direction is aligned with the ND, then other [100] directions will be exactly 90° away which gives rise to the smaller peak near 90°. The very sharp cube texture in this annealed condition is also associated with the development of a predominantly low angle boundary network as is seen from the GB map in Fig. 7b. The fraction of very low angle boundary with misorientation angle less than 5° (red) is 28.1 % while that of the boundaries with misorientation angle lying between 5° – 15° (dark blue) is found to be 67.4 %. The fraction of HAGBs (green) is only 4.5 % in this material. No visible presence of annealing twins could be identified in the microstructure.

It would be quite interesting at this stage to find out the origin of sharp cube texture after the ARB processing, particularly the relative contribution of the oriented nucleation and growth mechanisms [8]. For this purpose, small samples of the 8-cycle ARB processed sheets were lightly annealed at 300 °C for 15 s in a salt bath furnace, quenched immediately in cold water and subjected to EBSD measurements. The recrystallized volume fraction varied greatly between different EBSD scans due to the heterogeneous nature of nucleation of recrystallization. For statistical accuracy, data obtained from several EBSD scans were merged together and the average recrystallized volume fraction was determined from the merged dataset which was found to be ~15 %. However, only a few scans will be shown here where a number of recrystallized grains are identified. The recrystallized regions were separated

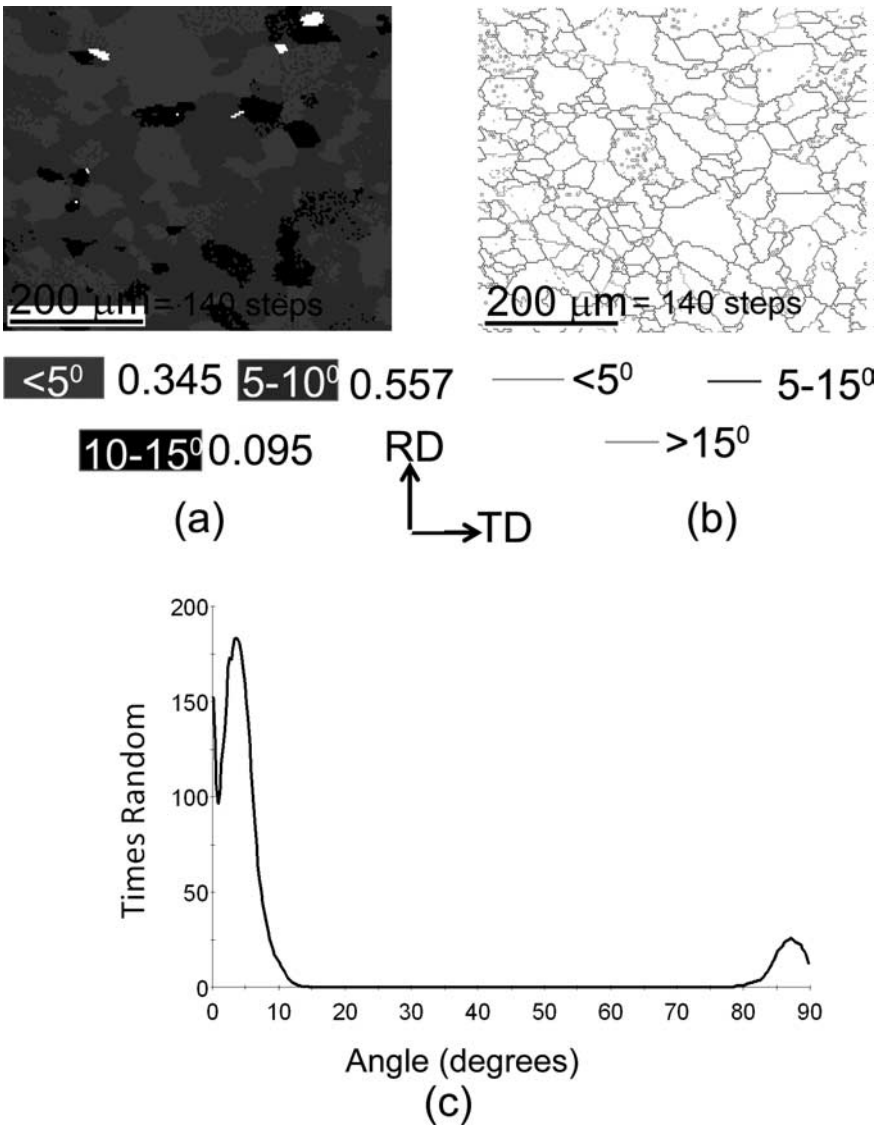

Fig. 7. (a) orientation map of the ARB processed Ni after annealing at 800 °C showing cube volume fraction at different misorientation from the exact cube. (b) is the GB map showing the distribution of grain boundaries with different misorientation angles (Colour online). (c) is the pole plot showing the quality of texture of the annealed tape.

from the deformed regions using a set of criterions that included

(i) internal average misorientation (Kernel Average misorientation (KAM) as defined in the TSL-OIM™ software [9]) should be less than 1°,
(ii) the grain size (by area) should be more than 4 μm^2 and
(iii) the regions must be bounded by HAGBs. A similar set of criteria have been used previously by Li et al. [10] and Bhattacharjee et al. [11] to isolate recrystallized regions from deformed regions in Ni.

Figure 8 shows the EBSD maps at early stages of recrystallization. Figure 8a and b corresponds to the rolling plane section and Fig. 8c and d correspond to the longitudinal plane. Figure 8a and 8c are the grain boundary maps and Fig. 8b and d depicts the orientation maps showing the recrystallized regions only. Evidently, most of the recrystallized grains in the rolling plane have sharp cube orientation (Fig. 8a and b). In the longitudinal plane section, however, few grains with orientations other than cube or rotated cube could also be identified. Figure 8e shows the (111) pole figure calculated from the recrystallized grains only. Development of a sharp cube texture at this early stage of recrystallization is quite evident from the appearance of the pole figure.

4. Discussion

The bulk and microtexture analyses by XRD and EBSD establish that pure Ni develops a homogeneous pure Cu or metal type deformation texture during the ARB processing. The microstructure of the as ARB processed material is a typical lamellar ultrafine microstructure which appears fairly homogeneous throughout the thickness of the sheet. By annealing at 300 °C, a strong cube texture develops in the material which is strengthened further with increasing annealing temperatures due to grain growth and after annealing at 800 °C nearly 100 % cube textured Ni tape could be obtained. The very sharp cube texture in the 800 °C annealed material is accompanied by the development of a predominantly low angle boundary network. Additionally, the recrystallized grains are free of annealing twins which should lead to the increase in intra- and inter-granular current transport in the epitaxial superconductor layer deposited on these substrates. These results clearly show that the ARB route has high potential for the use in fabricating highly textured coated superconductor substrate tapes.

The complete suppression of annealing twins in the microstructure of the SPD processed material in contrast to con-

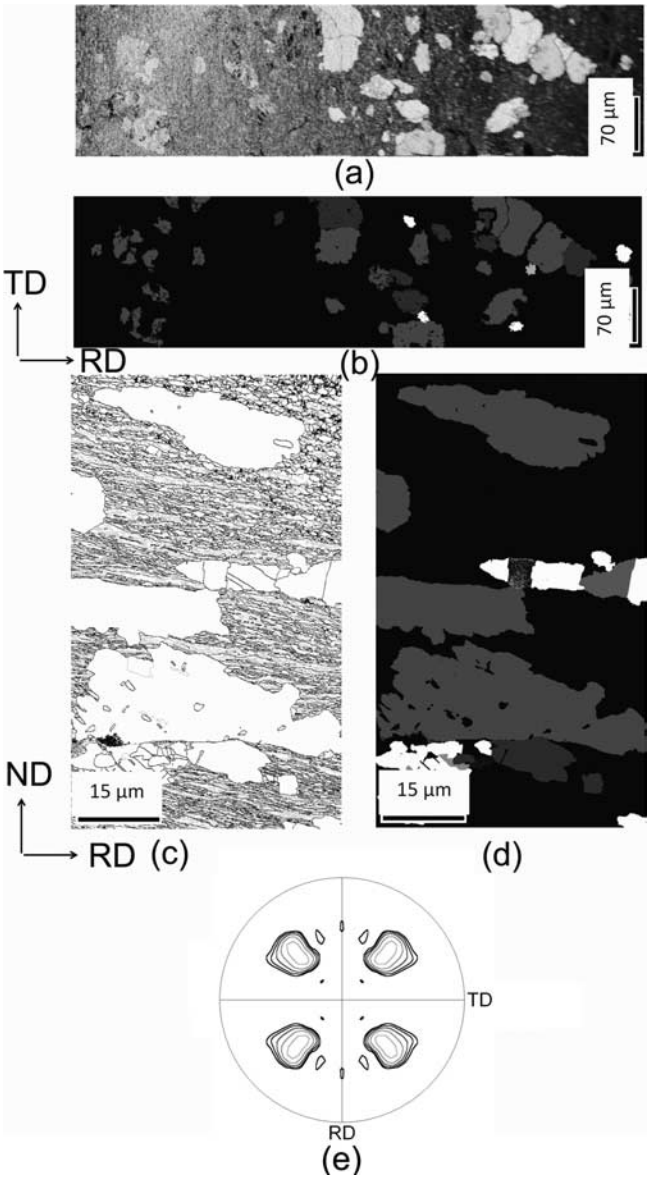

Fig. 8. (a) and (b) are GB and orientation maps of recrystallized fraction acquired from the rolling plane section of the ARB processed Ni annealed at 300 °C for 15 s. (c) and (d) are the GB and orientation maps acquired from the longitudinal section. (e) is the (111) pole figure calculated from the recrystallized fraction only. The color code for the orientation maps and intensity levels for the contour lines of the pole figure are same as in Fig. 1a and 1b, respectively. (Colour online)

ventionally deformation processed ($\sim$95 %) Ni with similar purity level is quite interesting [12]. In the low deformation regime the annealing twin density is found to increase with increasing prior cold working and the twin density is maximum at some intermediate value of strain [13]. In fact, low strain + annealing is a very effective route in increasing the special boundary fraction by controlling annealing twin formation in grain boundary engineered Ni and other materials [14]. Although, detailed analyses of annealing twin density in such severe deformation range have not been done so far, indications have emerged that twin density decreases with increasing rolling reduction [12] which is also consistent with the present observation of suppression of annealing twins in severely deformed Ni. Although the reason for the suppression of annealing twins is not quite clear at this stage but it appears that very high value of plastic strain imposed in the SPD process has a significant role to play. However, these issues need to be investigated further.

More interesting, however, is the origin of extremely sharp cube texture in such a severely strained material. In order to explain the origin of cube texture in medium to high stacking fault energy (SFE) fcc materials, two different models, namely, the oriented nucleation (ON) and oriented growth (OG) theories, have been proposed and debated for a long time [8]. According to the ON model, preferential nucleation of cube grains from pre-existing cube oriented regions is responsible for the development of a sharp cube texture. On the other hand, the OG model emphasizes that high mobility boundaries with certain misorientation relationship such as 40° ⟨111⟩ results in the selective growth of certain texture components. The cube component is found to maintain this relationship with the S orientation which is a major component of the deformation texture in fcc metals.

Turning our attention back to the present case, cube oriented regions, although quite scarce, are found in the deformed material which appearing as very thin bands extending to several micrometers in length along the direction of RD (Fig. 3b1). Orientation maps on the rolling and longitudinal plane sections at an early stage of recrystallization, however, show profuse cube oriented grains throughout the volume of the material, which far outweigh the miniscule presence of the cube volume in the deformed microstructure. The preferential nucleation of cube oriented grains clearly indicates the role of oriented nucleation in the development of cube texture in the ARB processed material. The preferential nucleation of cube grains, which has also been observed in other studies, is attributed to the special structure of cube bands characterized by their high orientation gradient, which offers a favorable environment for formation of a stable nuclei and early nucleation [11, 15] and an accelerated recovery of cube oriented subgrains due to the special arrangement of gliding dislocations inside the cube cells [16].

While the role of oriented nucleation is quite clear from the onset of recrystallization, the development of sharp cube texture is also aided by a definite growth advantage of the cube grains over grains of other orientations. This is quite clear from the values of average grain size ratio between cube to non-cube grains ($d_{\text{cube}}/d_{\text{non-cube}}$). The ration is found to be around 1.25 at early stages of recrystallization but increases to the 2.25 on the completion of recrystallization, indicating the growth advantage of the cube grains throughout the process of recrystallization. The growth advantage of the cube grains is continued after annealing at higher temperatures where the ratio is found to vary between 2.25–2.5. Similar values of $d_{\text{cube}}/d_{\text{non-cube}}$ during grain growth have been reported by Li et al. [10] for very high purity Ni, which agrees quite well with the observed growth advantage of the cube grains in this work. The textural evolution in the ARB processed material thus seems to be due to oriented nucleation of cube grains followed by the selective growth of these grains with progress of recrystallization due to the growth advantage of cube grains.

It may be noted that the mechanism of formation of cube texture in the severely strained ARB processed pure Ni does not differ to any significant extent as compared with conventional deformation processed medium to high

stacking fault energy fcc materials. The main observations in this study regarding the origin of sharp cube texture in the ARB processed material, i.e., oriented nucleation of cube grains followed by the selective growth of these grains with progressing recrystallization, agree quite well with the recent view on the mechanism of formation of cube texture in heavily rolled and annealed materials [3]. However, the ultrahigh strain imposed by the ARB process is significantly advantageous in enhancing the sharpness of the cube texture. The nearly 100% cube texture along with twin-free recrystallized microstructures observed after 8 cycles of ARB processing and annealing is not easy to attain in conventional deformation processing of Ni, where the strain value is much lower than that used in this work. The cube texture in conventional deformation processed Ni is quite often found to be imperfect, and usually a rotated cube component ($\{013\}\langle 100\rangle$) develops alongside the cube component during annealing which in some instances has been reported to be even stronger than the cube component. These characteristics may render the tapes unsuitable for coated superconductor applications [12, 17, 18].

While imparting very high levels of strain through ARB is quite beneficial for enhancing the strength of cube texture upon annealing as evident from the present study and also known from other work, the reasons are not very clear [3]. The deformation textures of both conventionally and ARB processed materials are quite similar and in both cases the cube volume fraction is negligible. It has been suggested previously that strain effect on cube texture formation is controlled by the spatial distribution of cube nuclei. In rolled materials the average spacing (λ) between nearest cube bands is proportional to $\exp(-\varepsilon)$ where ε is the rolling strain. It has been argued that if the λ value is comparable to the distance a cube grain can grow due to the difference in the nucleation time of the cube grain and grains of other orientations, the cube grains may grow without significant competition from other nucleating grains. In the present the cube bands were extremely scarce in the deformed microstructure and any statistically reliable data for the cube bands spacing could not be obtained. Nevertheless, these issues remain interesting and detailed microstructural analysis should be undertaken in future work to ascertain the reasons of enhanced strength of cube texture in severely deformed materials.

Since the starting thickness of the sheets remains nearly constant at the end of each ARB cycle (1 mm in this case), the final cycle should involve normal cold rolling to reduce the thickness of the sheets to a thin tape form. This would serve two additional advantages: Firstly this would increase the cross-section of the non-superconducting substrate layer and increase the critical current density (= current/total cross-sectional area, where total cross-sectional area is the sum of cross-sectional areas of metallic substrate, buffers and HTS layers) of the final coated conductor assembly. Secondly, this would further impart significant plastic strain to the already accumulated ARB strain, which is expected to further enhance the sharpness of the cube texture furthermore.

The ARB based route described in the present study should also be investigated for preparing highly textured, mechanically strong and non-magnetic nickel base alloy tapes such as Ni–W, Ni–Mo and Ni–Cr. The evolution of cube texture in these alloys during ARB processing and annealing should be the subject matter of a future study.

5. Conclusions

The following conclusions have been drawn from the present study:

1. Pure Ni develops an ultrafine microstructure through severe straining by ARB.
2. The deformation texture of the as-ARB-processed material is a typical pure metal or Cu type texture having strong presence of S, B_s and Cu components.
3. Cube oriented regions are present as long thin bands in the deformed microstructure although the volume fraction is almost negligible.
4. Sharp cube texture formation is observed upon annealing the ARB processed Ni sheets and a nearly 100% cube textured material having almost twin-free microstructure could be obtained by annealing at 800 °C.
5. The origin of sharp cube texture in the ARB processed material could be attributed to the oriented nucleation of cube grains followed by selective growth of the cube grains with progressing recrystallization.
6. Finally, ARB could be an effective route for preparing highly cube textured substrate tapes for coated superconductor applications.

The author would like to gratefully acknowledge the Japan Society for the Promotion of Science (JSPS) for supporting this work through the award of a postdoctoral fellowship under the auspices of which part of this work was carried out.

References

[1] A. Goyal, M.P. Paranthaman, U. Schoop: MRS Bulletin 29 (2004) 552.
[2] D. Dimos, P. Chaudhari, J. Manhart, F.K. Legoues: Phys. Rev. Lett. 61 (1988) 219. DOI:10.1103/PhysRevLett.61.219
[3] R.E. Smallman, C.S. Lee: Mat. Sci. Eng. A 184 (1994) 97. DOI:10.1016/0921-5093(94)91024-3
[4] N. Tsuji, Y. Saito, S.-H. Lee, Y. Minamino: Adv. Eng. Mater. 5 (2003) 338. DOI:10.1002/adem.200310077
[5] K. Pawlik, J. Pospiech, K. Lücke, in: Texture and Microstructures 14–18 (1991) 25. DOI:10.1155/TSM.14-18.25
[6] N. Hansen, D.J. Jensen: Philos. T. Roy. Soc. A 357 (1999) 1447. DOI:10.1098/rsta.1999.0384
[7] D.A. Hughes, N. Hansen: Philos. Mag. 83 (2003) 3871. DOI:10.1080/14786430310001605560
[8] R.D. Doherty: Mat. Sci. Eng. A 238 (1997) 219.
[9] S.I. Wright, D.P. Field, D.J. Dingley, in: A.J. Schwartz, M. Kumar, D.P. Field, B.L. Adams (Eds.), Advanced Software Capabilities for Automated EBSD, Academic/Plenum Publishers, New York (2000).
[10] X.L. Li, W. Liu, A. Godfrey, D.J. Jensen, Q. Liu: Acta Mater. 55 (2007) 3531. DOI:10.1016/j.actamat.2007.02.005
[11] P.P. Bhattacharjee, R.K. Ray, N. Tsuji: Acta Mater. 57 (2009) 2166. DOI:10.1016/j.actamat.2009.01.015
[12] H. Chang, I. Baker: Metall. Mater. Trans. A 38 (2007) 2815. DOI:10.1007/s11661-007-9324-1
[13] W. Charnock, J. Nutting: Met. Sci. J. 1 (1967) 78.
[14] S.L. Lee, N.L. Richards: Mater. Sci. Eng. A 390 (2005) 81. DOI:10.1016/j.msea.2004.08.044
[15] S. Zaefferer, T. Baudin, R. Penelle: Acta Mater. 49 (2001) 1105. DOI:10.1016/S1359-6454(00)00387-6
[16] A.A. Ridha and W.B. Hutchinson, Acta Metall. 1982 30 (1982) 1929. DOI:10.1016/0001-6160(82)90033-5
[17] R.K. Ray and P.P. Bhattacharjee: Philos. Mag. 87 (2007) 2417. DOI:10.1080/14786430701216269
[18] P.P. Bhattacharjee and R.K. Ray, Mat. Sci. Eng. A 459 (2007) 309. DOI:10.1016/j.msea.2007.02.087

(Received December 18, 2009; accepted November 9, 2010)

Bibliography

DOI 10.3139/146.110465
Int. J. Mat. Res. (formerly Z. Metallkd.)
102 (2011) 2; page 173 – 182

ISSN 1862-5282

Correspondence address

Dr. Pinaki Prasad Bhattacharjee
Assistant Professor
Department of Materials Science and Engineering
Indian Institute of Technology Hyderbad
Ordnance Factory Estate Yeddumailaram 502205
Andhra Pradesh, India
Tel.: +91 40 2301 6069
Fax: +91 40 2301 6003
E-mail: pinakib@iith.ac.in